

FEA based Dissipation Energy and Temperature Distribution of Rubber Bushing

Zhengui Zhang^a, Haiyan H Zhang^{*a}

^aMechanical Engineering Technology, Purdue University, West Lafayette, IN, US

Abstract

Rubber bushings used in the vehicle or aerospace can reduce the noise and vibration and absorb the shocks. The heat accumulation in the rubber components is attributed to the nonlinear mechanical behavior of rubber and leads to degeneration of mechanical properties. The viscoelastic damping is treated as the major mechanism of dissipation energy, which is heat source of temperature rising in bushing. A finite element method is expanded from elastic structure to viscoelastic structure and computes the dissipation energy distribution in the rubber core. Based on that heat source, the temperature distribution of rubber bushing under radial harmonic excitation has been calculated using finite volume method. The frequency and amplitude effect on dissipation energy and temperature distribution are described. The radial dynamic testing is carried out and the temperature is recorded using thermal imager to evaluate the simulation. As complement, the dynamic torsional testing is also carried out to explore the possible failure zone of rubber bushing under different types of loading.

Keywords: Rubber bushing; Viscoelastic; Finite element; Temperature; Dynamic testing.

I. Introduction

Rubber bushings installed on the automotive suspension system work as connecting components and isolator. Bushing can connect the small parts with the body of vehicle and also can minimize the transmission of noise and small vibration from a source to receiver[1]. Because of its elasticity and inherent damping, rubber bushings play a more and more important and critical role, especially, those engineering rubbers with carbon black fillers. Vehicles installed rubber components with better serving life have great advantages in the globally competitive market.

Compared with any other metal material used in the vehicle system, rubber has a higher capacity of energy storage. Rubber bushings are expected to be strong enough to undertake a certain loading and also high damping ability to reduce the vibration and noise. However, the basic disadvantage of high damping material is the thermal effect, which leads to fatigue and shortens components' serving life. Because of the nonlinear mechanical behavior of rubber, the stress- strain curve forms elliptical loop under cycle loading, which represents the energy dissipation and results in heat built up in the rubber products[2].

This heat accumulation is known as the primary reason of rubber degeneration after long time service, such as aging, hardening and damping losing and so on. The temperature of rubber bushing increases as the cumulative hysteretic energy and the much lower thermal conductivity of rubber material compared with steel. The self heating degenerated the mechanical properties of material and caused the

thermal failure of bushings[3]. Furthermore, the aforementioned temperature influence doesn't include the effect of chemical changes, which occurs due to aging or continuous vulcanization. The chemical processes of rubber are dependent on the temperature and those processes can stimulate the degradation of fatigue life at elevated temperature or long periods serving. In sum, the material properties are weakened, aging process is speeded, and the desired life expectation of rubber components is shortened due to the heat generated within the rubber[4].

As heat generation during service is a major concern of rubber components' lifetime, numerous researchers have investigated the heat generation mechanism, as well as the effect on mechanical properties and lifetime expectation. There are several mechanisms accounting for dissipation energy accumulated in rubber components. One reason is the hysteresis damping, which is dependent on strain amplitude, strain temperature and average strain range[5]. Hysteresis is small at low strain but maximized at high-strain and it can help the material retain its fracture toughness and fatigue resistance. Strain-crystallization and Mullins effect are two factors accounting for the hysteresis at high strain. The carbon black related rate-independent hysteresis and the rubber's viscoelastic lead to the hysteresis at low strain. The Mullins effect describes initial transient softening of rubber shown in the stress-strain curve before it reaches to a steady state, nonlinear response[6-8]. Strain crystallization takes place at higher strain and leads to increase of stiffness and hysteresis[9]. The time-dependent viscoelastic damping is another major mechanism accounting

for energy dissipation during deformation. The magnitude of energy loss in viscoelastic rubber is larger compared with the purely viscous behavior, which is associated with the mobility of molecular chains in polymer.

Many researchers investigated the temperature distribution in the rubber products with heat flow governing equations. Clark[10] developed a model to investigate the thermal equilibrium of pneumatic tire with solution about temperature. Later, with the development of the finite element method, thermal model has constructed on the basis of the finite stress and strain analysis, which was economically and reasonably to predict the heat distribution of the rubber components. Yeow[11] developed a three dimensional model and used the finite difference method to calculate the temperature distribution of tyre on the influence of various parameters. Becher[12] simulated the dissipation energy and temperature distribution of loaded tires using a rheological model combining the viscous Maxwell elements and plastic Prandtl elements. Those numerical approaches to predict the temperature distribution of tire during rolling assume the temperature independent deformation of structure. Yeong[13] carried out the FEA simulation to get the temperature of tire under dynamic condition using the experimental date about total strain energy and hysteresis energy loss. Actually, the bi-directional iteration was employed in some publications, in which the structure deformation and temperature are mutually affected [14-16]. That strategy to solve the temperature filed of rubber components has been widely accepted by many researchers. In sum, the mechanisms of heat generation in the viscoelastic material were discussed in many publications, especially the external excitation induced hysteresis damping[17]. One of the problems in predicting the temperature distribution is the proper the heat transfer model and heat transfer coefficients. Some of the researchers started from the surface temperature of rubber component to estimate the heat transfer coefficient of rubber, which results were close to the analysis solution[18, 19]. However, most of literatures focus the thermal behavior of the tire and few reports specified on the rubber bushing. As the critical role of rubber bushing and even longer expected service life compared with tire, the heat generation mechanism and temperature distribution is very important to evaluate the performance of rubber bushing. Furthermore, the linear viscoelastic model is much easier to be manipulated in the frequency domain rather in the time domain during the FEA program[20]. Thus, in this research, the FEA is employed to explore dissipation energy distribution of rubber

components under harmonic excitation. In this initial work, the one way structure-thermal coupling is adopted to simulate the temperature distribution without considering the temperature effect on the structure. With the temperature distribution obtained in this research, the heat concentration in rubber bushing can be identified, which is conducive to the design optimization.

The origination of this article is listed as follows. Part 2 elaborates the pre-processing and post processing of FEA program in dealing with viscoelastic structure. Especially, the calculation procedure of energy in each element is specified, including the potential energy, kinetic energy and dissipation energy. Before directly apply the FEA program to the dynamic analysis about rubber bushing, a simple clamped beam is tested in the Part 2. After the tentative verification with viscoelastic beam, Part 3 compares dissipation energy density of rubber core under radial harmonic excitation at different frequency and amplitude. Part 4 talks about the heat transfer simulation using the finite volume method to predict the temperature distribution of rubber bushing based on the heat source calculated in part 3.

Part 5 presents results of the experimental dynamic radial testing and torsional testing.

II. The Finite element program development

FEA can analyze complicated structure without simplifying to simple and general structure as doing in the theoretical analysis and that advantage makes it more powerful and applicable. Especially, with the development calculation capability of computer, the degree of freedom (DOF) of the structure is almost exponentially increased and corresponding solution becomes even more concisely elaborated. The incompressible 3-D viscoelastic solid is modeled with Hex20 element, which has 20 nodes and 60 DOF. Since the compounding ingredients and operating parameters affect the heat generation of rubber[21], the quantitative description of this material should be specified. Considering the limited experimental measurement for parameter identification and the real working environment of rubber bushing, the standard linear model is chosen as the constitutive model of rubber in the following FEA programming. Rubber coupon cut from the rubber bushing is used to identify the parameters of standard linear model and thermal properties. The parameters of the constitutive model are identified with the dynamic mechanical analyze (DMA), which give the spring and dashpot coefficients as $E_1=0.8$ MPa, $E_2=1.07$ MPa and $\eta=0.00323$ MPa.s in the frequency range 0-

100HZ[22]. The governing equation of forced damped vibration under harmonic excitation is written as[23],

$$[[K]+i\omega[C]-\omega^2[M]]\{\hat{u}\}=\{P\} \quad (1)$$

Where the $\{P\}$ is forcing function and $\{\hat{u}\}$ is the forced frequency response. The matrix in the bracket is the dynamic stiffness matrix $[\hat{K}_D]$, which is formed after the assembly of stiffness, mass, and damping matrix in the FEA program. The modulus of the viscoelastic structure is dependent on the modulus of the material, which is frequency dependent,

$$\hat{E}(\omega)=\left(\frac{i\omega\eta\left(\frac{E_1}{E_2}+1\right)+E_1}{E_1+i\omega\eta}\right)E_2=\phi(\omega)E_2 \quad (2)$$

With this frequency function of modulus, the FEA program developed for elastic structure can expand to viscoelastic structure and termed as Simplex program in following discussion. For convenience, the modulus of rubber is set as 1MPa in the definition of material properties. And then, multiply the dynamic stiffness $[K]_0$ of the viscoelastic structure with the frequency function $\phi(\omega)E_2$. Since the initial real variable $[K]_0$ turn to complex variable $[\hat{K}]$ after this treatment, the numerical solutions are complex variables. The displacement of each node is composed of two components,

$$\begin{aligned} \mathbf{u} &= [\mathbf{u}_R + i\mathbf{u}_I]e^{i\omega t} \\ &= [\mathbf{u}_R \cos(\omega t) - \mathbf{u}_I \sin(\omega t) + i[\mathbf{u}_R \sin(\omega t) + \mathbf{u}_I \cos(\omega t)]] \end{aligned} \quad (3)$$

With the displacements at each node, the stress and strain can be calculated from the quadratic hexahedral interpolations. Figure 1 gives the sketch of the 27 integration points used in the Simplex program.

$$\boldsymbol{\varepsilon} = [\boldsymbol{\varepsilon}_R \cos(\omega t) - \boldsymbol{\varepsilon}_I \sin(\omega t)] + i[\boldsymbol{\varepsilon}_R \sin(\omega t) + \boldsymbol{\varepsilon}_I \cos(\omega t)] \quad (5)$$

$$\boldsymbol{\sigma} = [\boldsymbol{\sigma}_R \cos(\omega t) - \boldsymbol{\sigma}_I \sin(\omega t)] + i[\boldsymbol{\sigma}_R \sin(\omega t) + \boldsymbol{\sigma}_I \cos(\omega t)] \quad (6)$$

With the strain and strain, the dissipation energy of this system is ready to calculate. The energy equilibrium of a system under external load is given as,

$$W - U - \tau = D \quad (7)$$

Where W is the work done by the external force, U is the strain energy stored in the system, τ is the kinetic energy stored in the system and D is the dissipation energy. In each cycle, the kinetic energy and strain energy are conservative and do not contribute to energy accumulation or dissipation. Thus, to keep the energy conservation, the energy obtained from the external load should be equivalent to the dissipation energy calculation from the loop area forming by strain and stress. In the Simplex program, the loading $p_i(t)$ and the corresponding

The strain and stress of the 27 integration points in each element can be obtained from the displacement of the 20 nodes in each element.

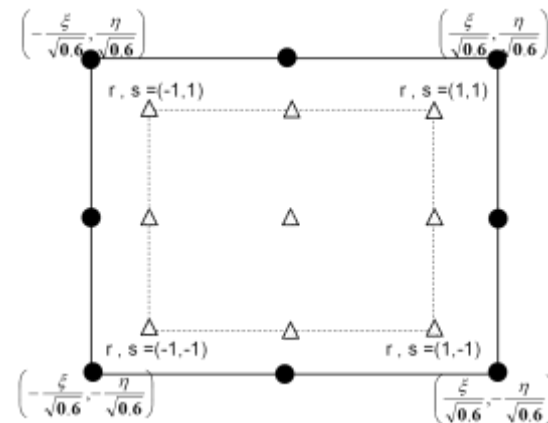


Figure 1. Integration points inside the Hex20 element. The sampling weights points and weights for Gauss Lagrange quadrature are

$$\begin{aligned} \mathbf{r}_i = \mathbf{s}_i = \mathbf{t}_i &= [-\sqrt{0.6} \quad 0 \quad \sqrt{0.6}] \quad \text{and} \\ \mathbf{W}_i &= [-5/9 \quad 8/9 \quad 5/9]; \quad \text{That gives } r = \xi/\sqrt{0.6}, \\ s &= \eta/\sqrt{0.6} \quad \text{and } t = \zeta/\sqrt{0.6}. \quad \text{The strain and stress at} \\ &\text{each node can be extrapolated using the Equation 4,} \\ \boldsymbol{\varepsilon}_i &= \sum_{p=1}^{27} N_p(r, s, t) \boldsymbol{\varepsilon}_p \quad \text{and} \quad \boldsymbol{\sigma}_i = \sum_{p=1}^{27} N_p(r, s, t) \boldsymbol{\sigma}_p \end{aligned} \quad (4)$$

Where, $N_p(r, s, t)$ is the shape function; $\boldsymbol{\varepsilon}_p$ and $\boldsymbol{\sigma}_p$ are strain and stress of each integration point. In this approach, multiple stress and strain have been assigned to those nodes shared by two or more elements. To solve this problem, nodal strain and stress are averaged to produce a smooth distribution. The complex stress and strain at each interpolation point are represented as,

displacement $u_i(t)$ of each node are collected. The increment of displacement at each time step is $du_i(t) = u_i(t) - u_i(t-1)$, and the work done by the external load at each node can calculate from the summation over $p_i(t) du_i(t)$ in the time domain. The summation of loop area calculated from each pair of the force and displacement is the total external work done to the system.

In the structure made of elastic material, the strain energy is related to the displacement square or strain square. For the simple spring and mass system, the strain energy can be easily estimated through $1/2 Ku^2$. Nevertheless, in a structure with viscoelastic material, square of the displacement does not mean the magnitude of the response because the

displacement is complex. The general expression of the strain energy in each element is given as,

$$U = \frac{1}{2} \int_{V^0} \{u\}^T [B_L]^T [D][B_L] \{u\} dV^0 \quad (8)$$

While it is not convenient to calculate the dV^0 since the mesh is not uniform for some complicated structure, thus, the isoparametric volume is recommended to replace dV^0 as

$dV^0 = |J_e| dr ds dt = |J_e| dV_c$, where J is the Jacobian matrix. Therefore, the strain energy of the element turns to,

$$U = \frac{1}{2} \{u\}^T \int_{V^0} [B_L]^T [D][B_L] J_e | dV_c \{u\} \quad (9)$$

As to the Hex20 element, the complex strain of the 27 interpolation points are derived from $u * B_L$ and the complex stress σ of the 27 interpolation points are derived using $u * B_L * D$. Where D is the stress-strain matrix and B_L matrix of Hex20 is,

$$[B_L] = \begin{bmatrix} A_x & 0 & 0 \\ 0 & A_y & 0 \\ 0 & 0 & A_z \\ A_y & A_x & 0 \\ 0 & A_z & A_y \\ 0 & 0 & A_x \end{bmatrix}_{I=1,N}, \text{ and} \quad (10)$$

$$\begin{Bmatrix} u_x \\ u_y \\ u_z \end{Bmatrix} \equiv \begin{bmatrix} A_x \\ A_y \\ A_z \end{bmatrix}_{I=1,N}$$

The dissipation energy at each interpolation point displays from plotting the real part of stress against real part of strain, which are extracted from the complex stress and strain. Similarly, the strain $\varepsilon(t)$ and stress $\sigma(t)$ shows the existence of phase delay and the loop area formed in each integration point can be calculated from,

$$Diss = \int_{t=0}^{t=1/2\pi f} \sigma(t) d\varepsilon(t) \quad (11)$$

It is important to point out that strain and stress in Equation 11 are real components since only the real parts of the stress and strain are extracted at the very beginning of the calculation. The integral of the product of stress and strain in time domain gives the dissipation energy in one integration point and the summation over the 27 interpolation points represents the dissipation energy of a Hex20 element.

To calculate the potential energy using the Simplex program, the real part of the displacement of each node in the Hex20 element is extracted. Potential energy of the Hex20 element is simply written as,

$$U = \frac{1}{2} \{u\}^T [k] \{u\} \quad (12)$$

The stiffness matrix $[K]$ of each element is,

$$[k] = \int_{V_c} [B_L]^T [D][B_L] J_e | dV_c \quad (13)$$

With the definition of stiffness matrix in Simplex, the time dependent strain of the 27 interpolation points are obtained by multiplying displacement with matrix B_L . Then, the time dependent stress of the 27 interpolation points are obtained by multiplying strain with matrix D . The summation of the product of stress and strain at the 27 interpolation points is the total potential energy in each Hex20 element.

The kinetic energy calculation is based on the mass matrix of Hex 20 element, which is formed as,

$$m_{ij} = \int_{V_c} \rho h_I(r,s,t) h_j(r,s,t) J_e | dV_c \quad (14)$$

With the lumped mass of each node, the kinetic energy is directly calculated from the square of the real part of the velocity multiplying half of the lumped mass. To verify the energy conservation of the system, the kinetic energy of the whole system is summed up over all nodes. The real part velocity comes from the complex displacement at each node,

$$v = -\omega u_R \sin(\omega t) - \omega u_I \cos(\omega t) \quad (15)$$

To test the reliability of the Simplex program in developing the dissipation energy, a clamped beam is practiced before analyzing the more complicated cylindrical rubber bushing. The viscoelastic beam is meshed into 40 elements and vertical harmonic loading force is applied on the central line of the structure. The frequency scan gives the first damped natural frequency as 33.5Hz. With the Simplex program, the external work done on the clamped beam, potential energy, kinetic energy and dissipation energy (strain energy) of the viscoelastic structure at different excitation frequency are calculated. Figure 2(a) shows the accumulated work, the dissipation energy, potential energy and kinetic energy in one cycle at 1HZ and 45 HZ. The structure experiences deformation slowly under the quasi-static excitation at 1HZ.

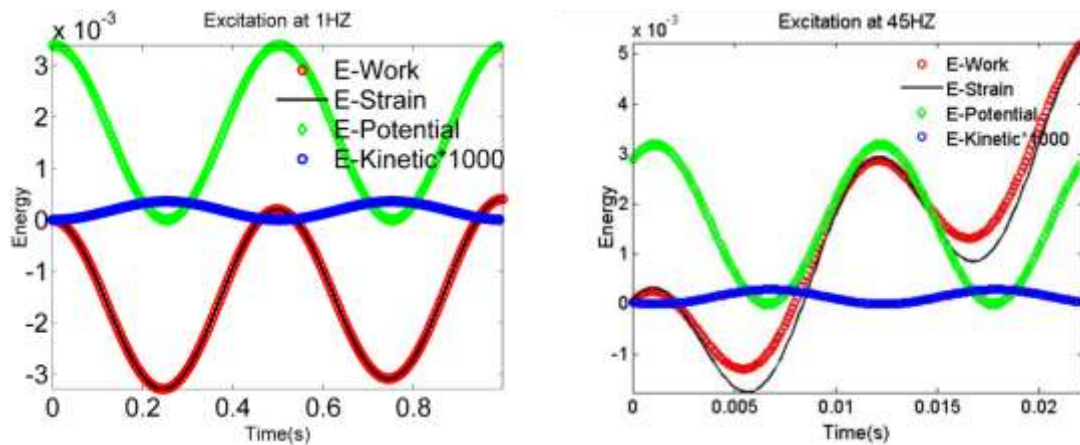


Figure 2. Energy accumulation at 1HZ and 45HZ.

Kinetic energy is quite small compared with others since the velocity of the nodes is fairly slow under low frequency excitation. Thus, a scale 1000 is multiplied to enlarge the variables of kinetic energy in the plot. The potential and kinetic energy variation change in time domain but the ending value is consistent with beginning value after one cycle. Because excitation at 1HZ is approximated to the quasi-static deformation, the different between the ending value of dissipation energy and beginning value is very small after one cycle. But the external work calculated from the loading and the corresponding displacement at central zone of beam overlaps with the dissipation energy accumulation in time domain. Figure 2 confirms energy conservation in the system and verifies the accuracy of Simplex program development. Figure 2(b) explores the frequency effect on dissipation energy and the result indicates that the excitation at 45HZ accumulated

much faster and higher than that at 1HZ. As expected, the kinetic energy and potential energy are still conservative after one cycle and the integral of dissipation energy follows with the variation of external work accumulation.

Figure 3 shows the periodicity of dissipation energy under harmonic excitation. The derivative of external work and dissipation energy over time are plotted as $dt(work)$ and $dt(strain)$. No matter under excitation 1HZ or 45HZ, the curve of $dt(work)$ and $dt(strain)$ are sinusoidal function. Then, the external work and dissipation energy built up are definitely periodic because they are calculated from the integral of periodic function. With this principle, the heat generation rate of a structure under harmonic excitation is a constant if the thermal effect of the structure is ignored.

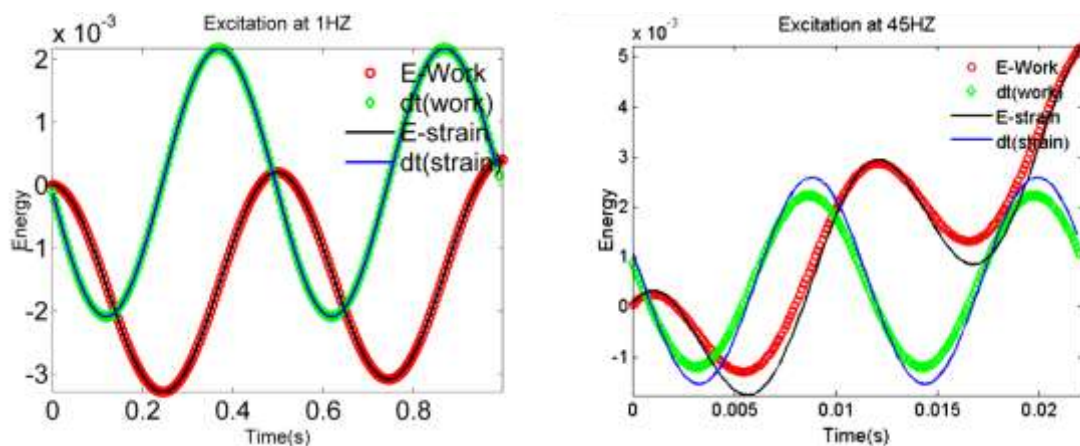


Figure 3 Periodicity of the external work and strain energy (dissipation energy).

III. The dissipation energy density in rubber bushing

Figure 4 (a) shows the nonuniform displacement of rubber core under the vertical loading force applied at the outer surface of the rubber core to simulate the dynamic tensile test. The inner surface

of the rubber is attached with the steel shaft and treated as fixed boundary in the model. The real part and magnitude of displacements decrease from the outer surface to the inner surface of rubber core. Figure 4 (b) shows the frequency dependence of the displacement. The node at the top of the bushing has

been selected. Because of the high natural frequency of the viscoelastic cylindrical rubber bushing, the frequency effect at lower frequency is dominated by the properties of viscoelastic material rather than the resonance effect. Thus, with the increase of module

with the frequency, the real part and magnitude of the displacement decrease. The peak value of imaginary displacement under frequency scan is corresponding to the damping behavior of the material used in this simulation.

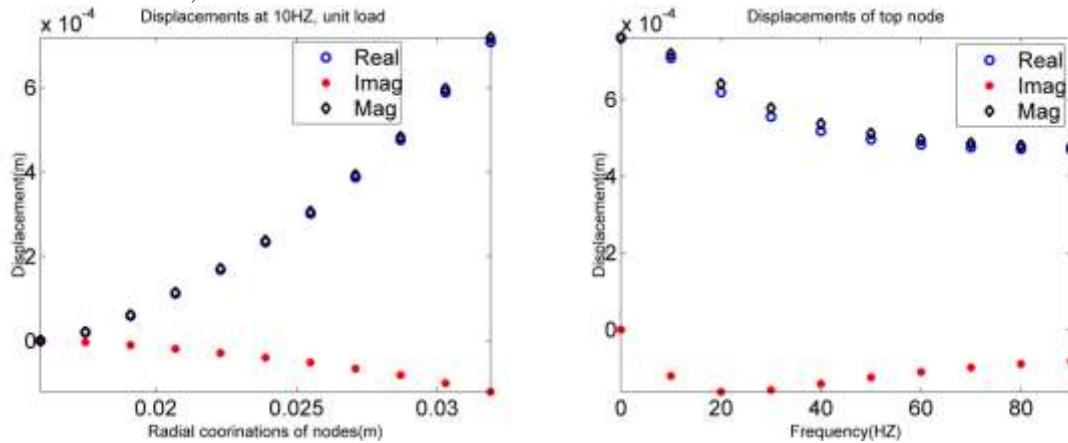


Figure 4. Displacements (a) Nodes arranged in radial from low to high position; (b) top node at different frequency.

Figure 5 shows the dissipation energy distribution of rubber core at excitation frequency 10HZ. Since the top node has the maximum displacement, the displacement of the top node is taken as the excitation amplitude. The highest dissipation energy density appears at the top and bottom loading zone of the rubber bushing. When the

excitation amplitude is doubled to 2mm, the magnitude of dissipation energy increases a lot while the distribution is kept. The dissipation energy distribution in radial direction is similar to the tendency of displacement. Combining the amplitude effect, it is clear that the higher the displacement, the higher is the accumulated dissipation energy.

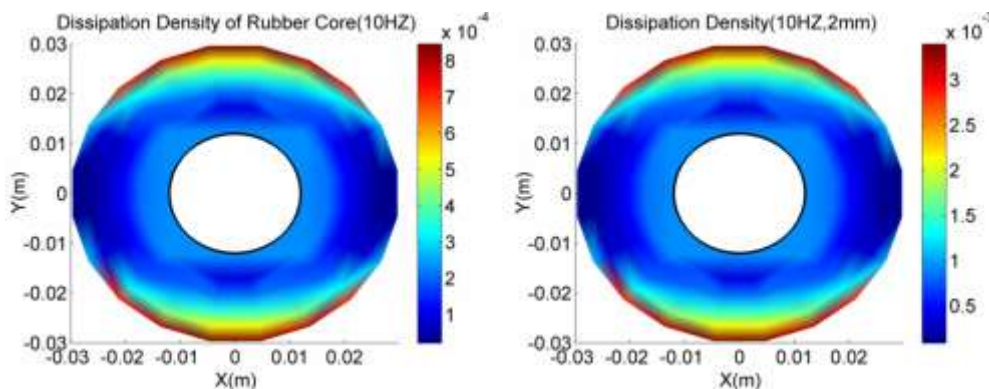


Figure 5. Density of dissipation energy in rubber core (a) Amplitude=1mm; (b) amplitude=2mm.

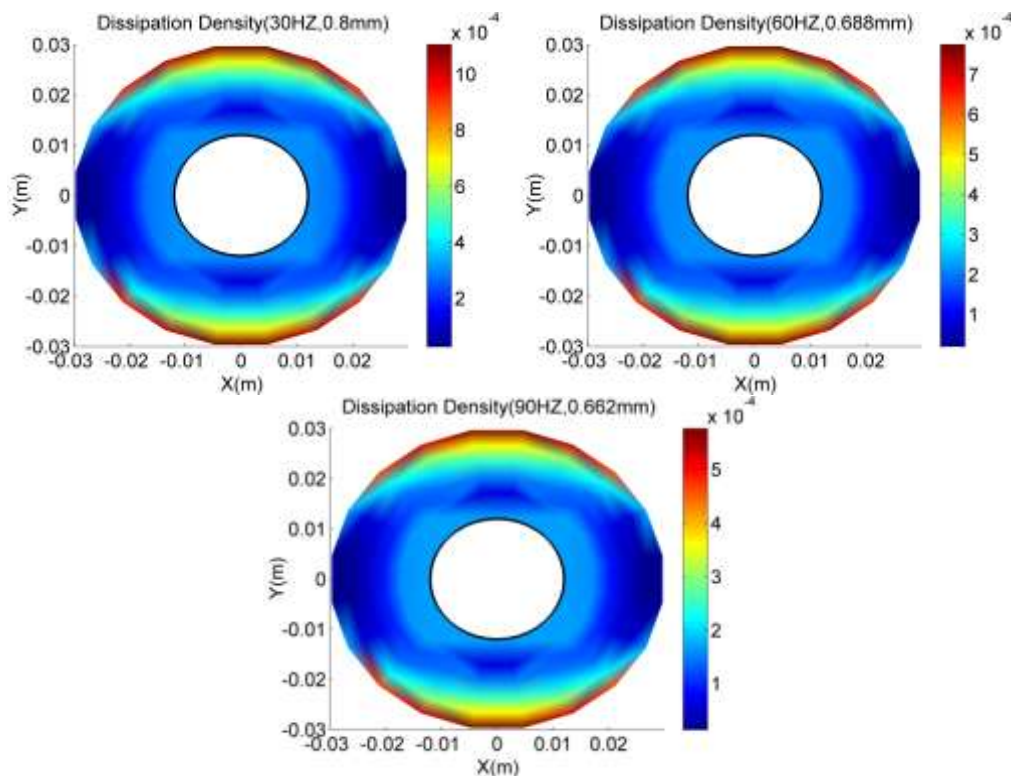


Figure 6. Density of dissipation energy in rubber core (a) 30HZ; (b) 60HZ; (c) 90HZ.

Figure 6 displays the frequency effect on the magnitude of dissipation energy. In this testing range of frequency, the DMA test on rubber coupon shows monotonously increase of modulus. Thus, under the same loading force, the amplitudes decrease at rising excitation frequency. That effect results in 1mm, 0.8mm, 0.688mm and 0.662mm amplitude at 10HZ, 30HZ, 60 HZ and 90HZ excitation respectively. The fast increase of modulus happens below 60HZ in current material and the modulus approaches to constant when excitation frequency approximates to 100HZ. From 10HZ to 30HZ, the stiffness of the structure changes significantly and leads to almost 20% reduction of amplitude. Nevertheless, after 60HZ, the slowly increase of modulus just slightly affects the stiffness and has little effect on the excitation amplitude.

IV. The numerical temperature distribution

The stress-thermal analysis is based on the assumption that the mechanical properties of linear viscoelastic material is temperature independent, as thermo-rheologically research about the rubber is needed if dealing with the temperature dependent material[24]. The heat conductivity and other thermal properties are measured using the hot disk thermal analysis instrument, which is based on the transient plane source (TPS) method. The specific heat and heat transfer coefficients are estimated using the rule of mixture assuming the compositions of rubber are carbon black and polymer and neglecting the trivial components. The physical and thermal properties of rubber used in this research are given in Table 1.

Table 1: Physical properties of rubber

Properties	Poisson's ratio	Heat transfer coeff	Static Modulus
Value	0.495	10(W/(m ² .K))	0.01(GPa)
Heat Capacity	Thermal diffusivity	Density	Thermal conductivity
1611.44(J/Kg.K)	0.202(mm ² /s)	952.54 (Kg/m ³)	0.343(W/m.K)

There are some assumptions about the heat transformation simulation on rubber bushing. Firstly, heat source of rubber bushing comes from the frequency dependent viscous damping. Secondly, the outer surface of the steel sleeves is exposed to

ambient air at room temperature. The heat convection is the main approach to transfer the heat from rubber bushing to air. Thirdly, the inner steel sleeve is installed on the balancing bar of the suspension system and the heat transform from the inner surface

is relative slow. Finally, the cross section of the rubber bushing is modeled considering the negligible heat transfer in axial direction. The mesh of the

rubber core tallies with FEA element distribution in the process of dissipation energy calculation.

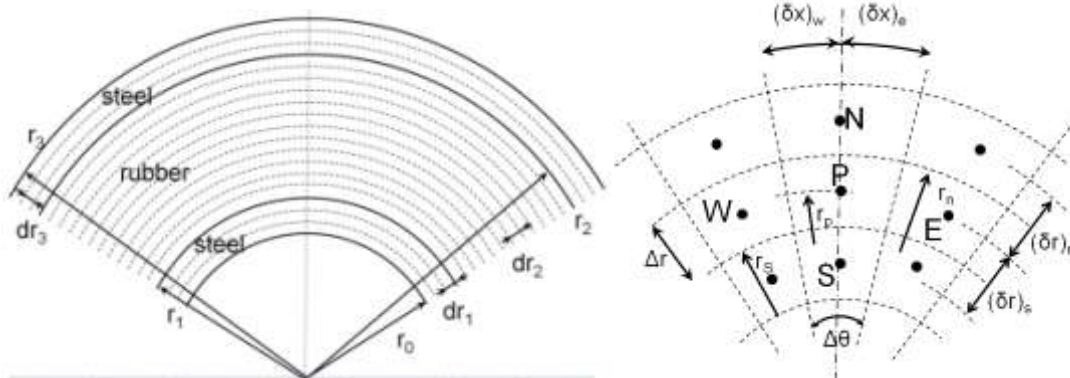


Figure 7. (a) Sketch the radial mesh of rubber bushing; (b) control volume

Figure 7(a) is part of the radial mesh of rubber bushing and Figure 7(b) is the control volume of rubber. The governing equation of transient heat transfer problem in the cylindrical coordination system is written as,

$$\rho c \frac{\partial T}{\partial t} = \frac{\partial}{\partial x} \left(\lambda \frac{\partial T}{\partial x} \right) + \frac{1}{r} \frac{\partial}{\partial r} \left(r \lambda \frac{\partial T}{\partial r} \right) + S \quad (16)$$

According to the definition of control volume, heat transfer governing equations of current rubber bushing are classified into three cases. The first governing equation applies to control volume inside of rubber,

$$a_p = a_E + a_W + a_N + a_S + a_p^0 - S_p \Delta V \quad (17)$$

$$\left(a_p - a_n + \frac{\Delta_r}{1/h + (\delta r)_n / \lambda_n r_n} \right) T_p = a_E T_E + a_W T_W + \frac{T_f}{1/h + (\delta r)_n / \lambda_n r_n} \Delta_r + a_S T_S + b \quad (18)$$

Where $b = S_p \Delta V + a_p^0 T_p^0$. The third control volume describes the thermal equilibrium between the interface of rubber and steel. As to rubber at the interface, the governing equation in Equation 17 still applicable after replacing the coefficients to

$$a_p^0 = \frac{((\rho c)_n + (\rho c)_s) \Delta V}{\Delta t} \quad \text{and}$$

$\Delta V = 0.5(r_n + r_s) \Delta r \Delta x$. Whereas the governing equation of the steel is changed to Equation 19 since the heat built up in the steel is negligible and treated as zero,

$$a_p = a_E + a_W + a_N + a_S + a_p^0 - S_p 0.5(r_n + r_s) \Delta r_s \Delta x \quad (19)$$

Where $b = S_c 0.5(r_n + r_s) \Delta r_s \Delta x + a_p^0 T_p^0$.

With the dissipation energy generation rate estimated from the Simplex program, the temperature distribution at the cross section of rubber bushing becomes available. Figure 8 shows the temperature

Where $a_E = \frac{r_p \Delta_r}{(\delta x)_e / \lambda_e}$, $a_W = \frac{r_p \Delta_r}{(\delta x)_w / \lambda_w}$,
 $a_n = \frac{r_n \Delta_x}{(\delta r)_n / \lambda_n}$, $a_s = \frac{r_s \Delta_x}{(\delta r)_s / \lambda_s}$,
 $a_p^0 = \frac{(\rho c)_p \Delta V}{\Delta t}$,

and $\Delta V = 0.5(r_n + r_s) \Delta r \Delta x$. The second governing equation applies to the control volume at the boundary between the steel sleeves and air,

rising on the cross section after different loading period and the excitation at 10HZ is chosen according to a field test about rubber bushing installed on the exhaust system. The temperature of rubber core increases obviously with the constant self heating rate. The plots indicates that the maximum temperature of rubber bushing changes from 315K, 330K, and 340K to 350K after loading time 600s, 1800s, 3600s and 7200s. The thermal conductivity of steel is 10 to 100 times higher than that of rubber. As a result, the temperature gradient in the steel is much lower than rubber's, and the later shows much higher temperature at the top and bottom loading zone than the middle area. The author tries to assign the thermal conductivity of rubber with a number 10 times higher than the measured value and the temperature gradient in rubber core is highly reduced. However, the low heat transfer coefficient and thermal conductivity of rubber definitely causes the heat and temperature rising concentrated in certain area.

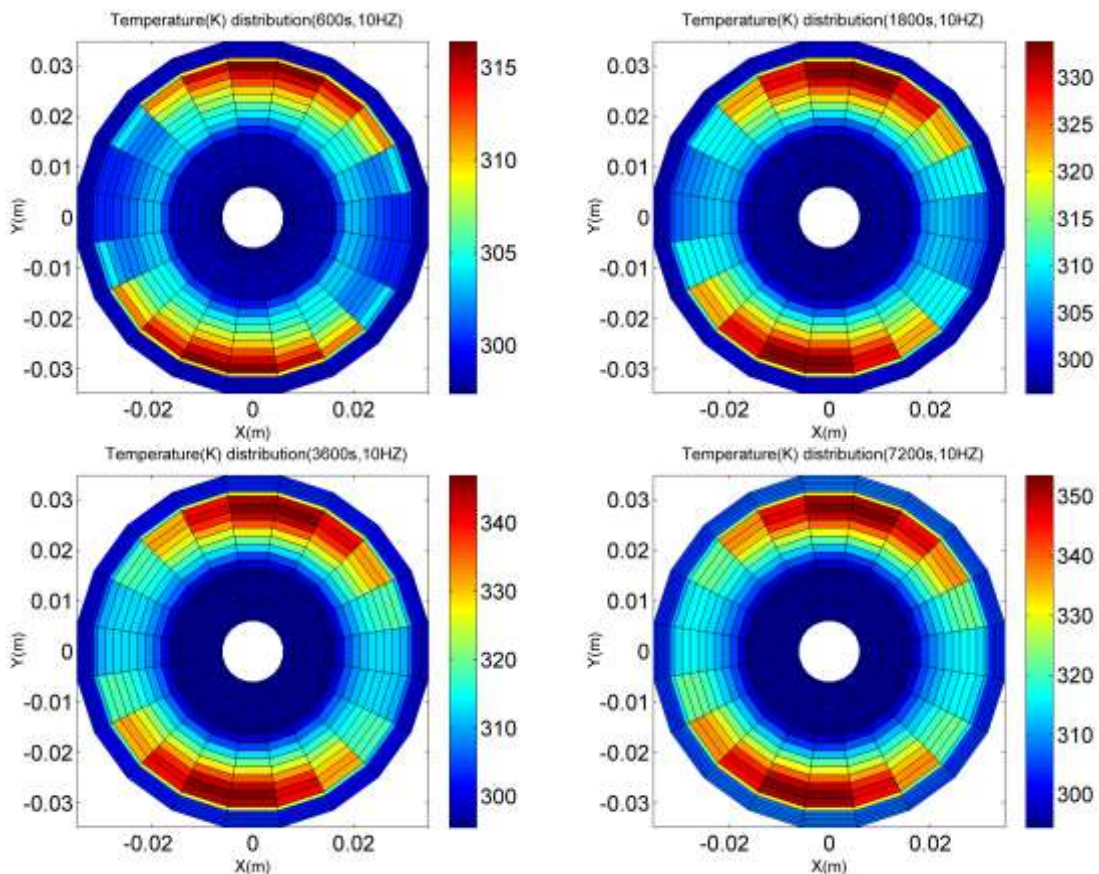


Figure 8. Surface temperature distribution of the rubber bushing at 10HZ; (a) 600s; (b)1800s; (c)3600s; (d) 7200s.

The amplitude effect on the temperature distribution of rubber bushing at 10HZ excitation is given in Figure 9. After 120s, 1mm amplitude excitation leads to the maximum temperature 303K while the 2mm amplitude excitation displays a maximum temperature 315K. Figure 8(a) indicates

that 600s is needed to reach that temperature 315K if the excitation is applied with 1mm amplitude. Thus, this comparison may imply a short service life of rubber bushing under larger deformation since the temperature increases much quickly in that case.

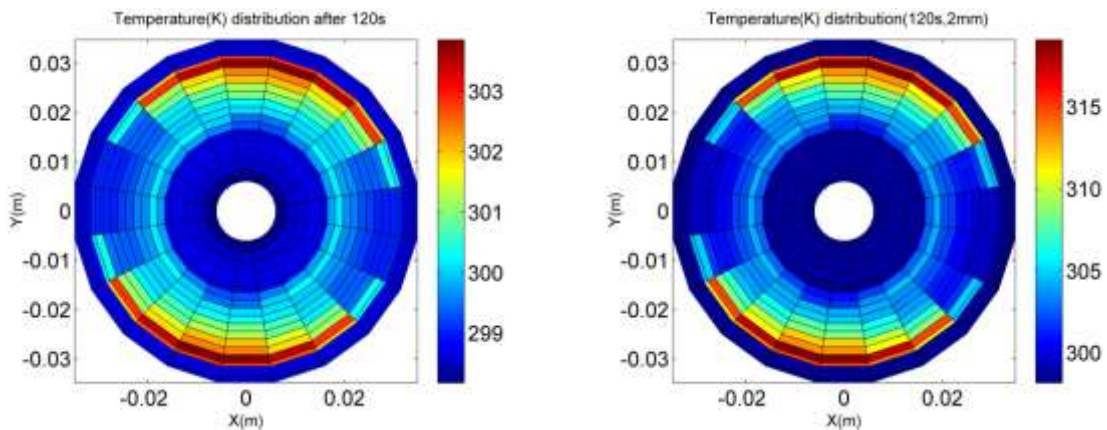


Figure 9. Temperature distribution of rubber at amplitude (a) 1mm; (b) 2mm.

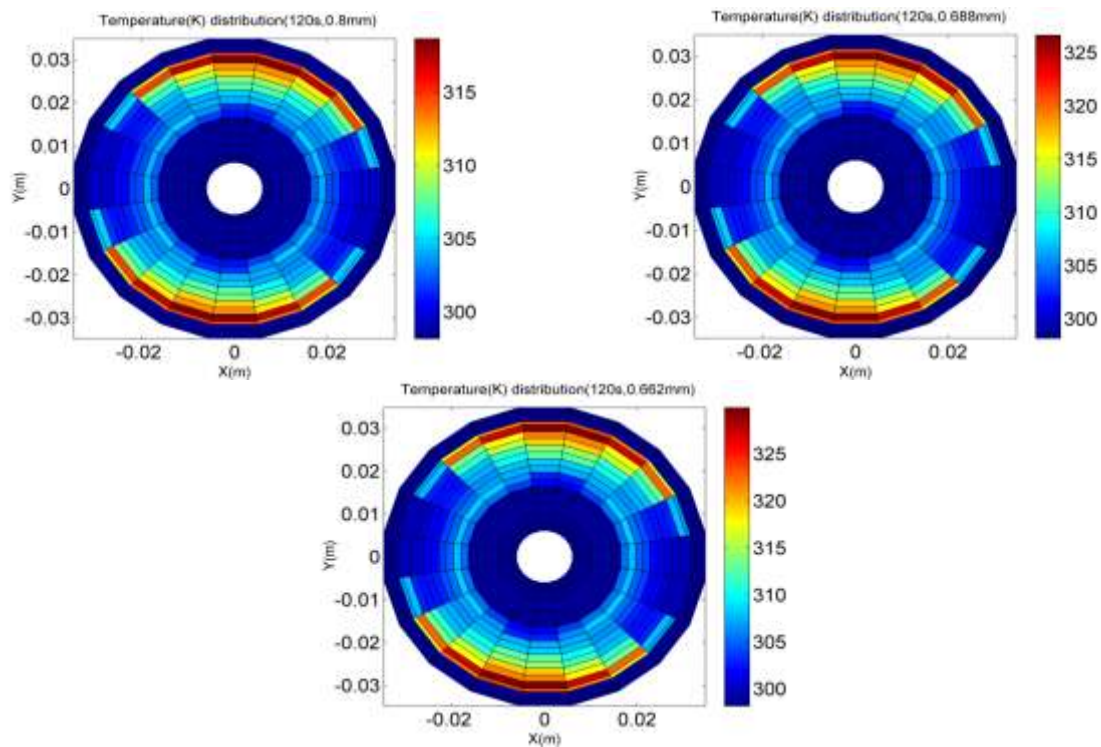


Figure 10. Temperature distribution at frequency (a) 30HZ; (b) 60HZ; (c) 90HZ.

The frequency effect on temperature rising inside of rubber bushing is presented in Figure 10.

Because of the increasing modulus of rubber material in the test frequency range, especially the big increase in the range 0~45HZ, the amplitude decreases from 0.8mm, 0.688mm to 0.622mm as the excitation frequency increases from 30HZ, 60HZ to 90HZ. Thus, the temperature distribution of rubber bushing after 120s as shown in Figure 10 should combine the influence of frequency and amplitude. The higher frequency means more cycles in unit time while the corresponding low amplitudes leads to lower dissipation energy in per cycle. As a result, the excitation at 60HZ presents apparent increase of temperature compared with that at 30HZ, however, the excitation at 90HZ gives a close temperature as the 60HZ excitation due to the comprehensive effect of amplitude and frequency. If the modulus of material is frequency dependent, the higher frequency definitely causes more dissipation energy and higher temperature.

V. Dynamic testing

With the Simplex program and heat transfer simulation, the temperature distribution of rubber bushing under vertical dynamic loading with different excitation frequency and amplitude are predicted. To verify reliability of the numerical calculation, the dynamic radial testing is carried out to compare with the simulation results. Torsional dynamic test is also required since torsional loading is one of the major loading types of rubber bushing and that result is significant to explore the failure mechanism. However, the MTS equipment has restricted specification about the dimension of samples in order to fit them into the clamps. The fixtures prepared for radial and torsional dynamic testing are designed and machined. Figure 11(a) is the original profile of rubber bushing and Figure 11(b) and (c) are fixtures incorporating the bushings for radial test and torsional test.



Figure 11 (a) Rubber bushing; (b) tension/compression fixture; (c) Torsion fixture

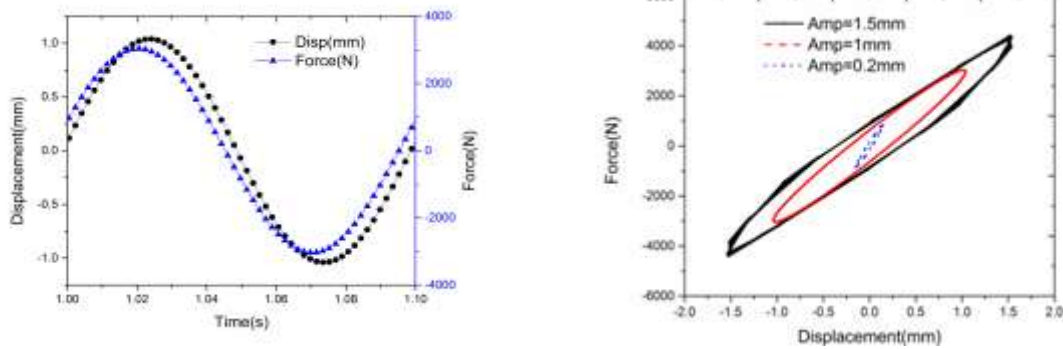


Figure 12. Dynamic radial test (a) Out of phase at 10HZ and amplitude 1mm; (b) the amplitude dependence of the stiffness at 10HZ.

The sinusoidal signal is chosen for the dynamic test and the input amplitude and frequency of each loading is specified. To have apparent temperature variation in a few minutes, the amplitude should be at least 1mm and the test range of the instrument is no more than 2mm. The recorded time for each case is dependent on the time required to have at least three steady cycles. The temperature rising of rubber bushing during the dynamic test is recorded using the thermal imager. The environment temperature of the

dynamic testing is about 298K. Figure 12(a) plots the phase shift between displacement and force at excitation at 10HZ and 1mm amplitude. Figure 12(b) records the influence of amplitude on the dynamic stiffness of rubber bushing. The dynamic stiffness at amplitude 0.2mm is higher than that at 1mm and 1.5mm. The tendency indicates that increasing the excitation amplitude leads to the softening of rubber components.

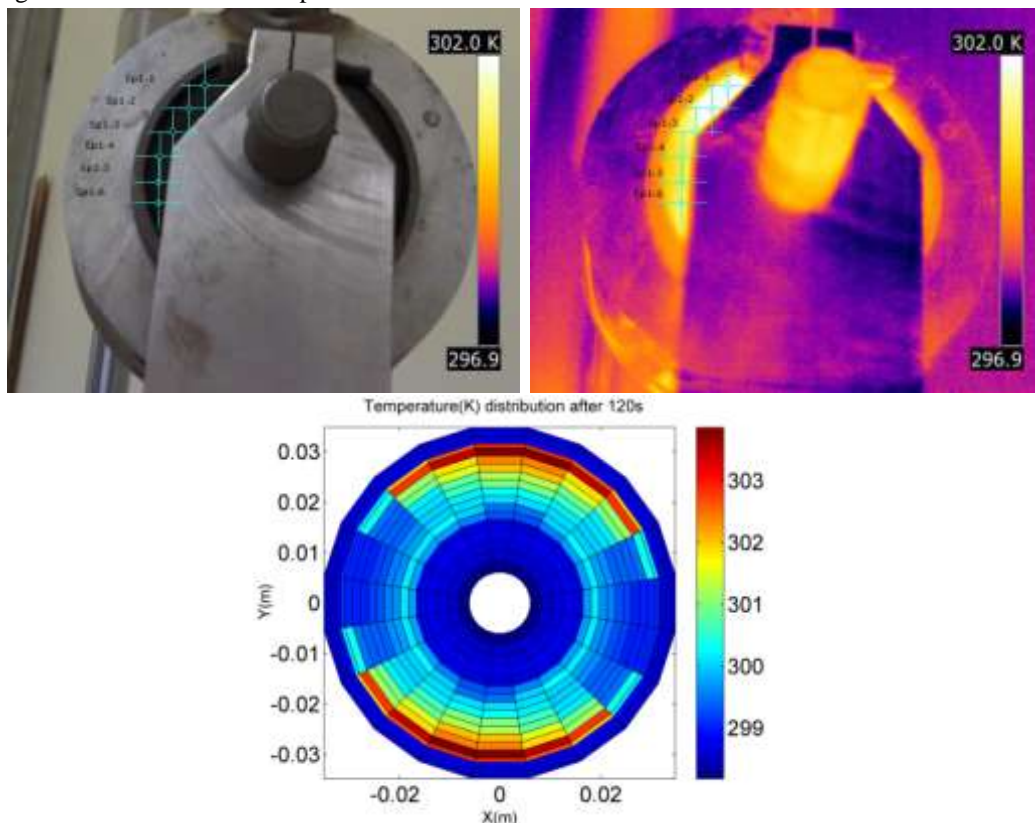


Figure 13. Temperature distribution on the surface of rubber core (a) Digit camera; (b) thermal; (c) numerical simulation.

Figure 13 compares the temperature distribution obtained from the dynamic testing with the heat transfer simulation. Because of the special design of

the fixture, only part of the surface of rubber bushing can be photographed using the thermal imager. The temperature shown in Figure 13 is the rubber bushing

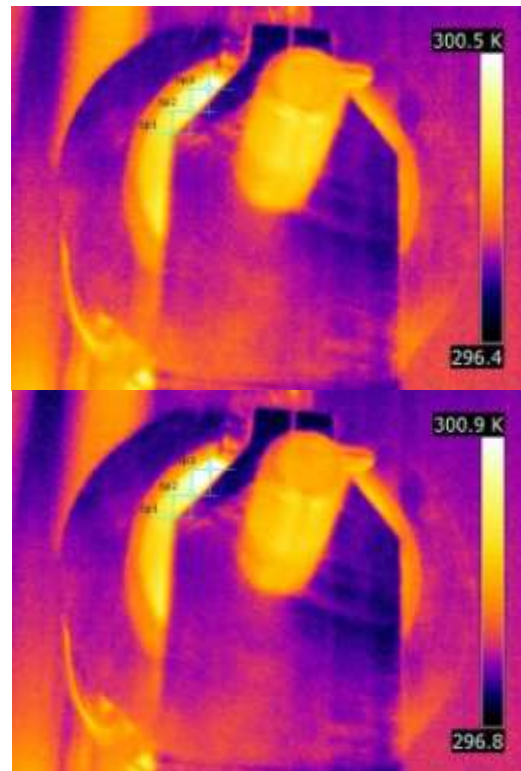
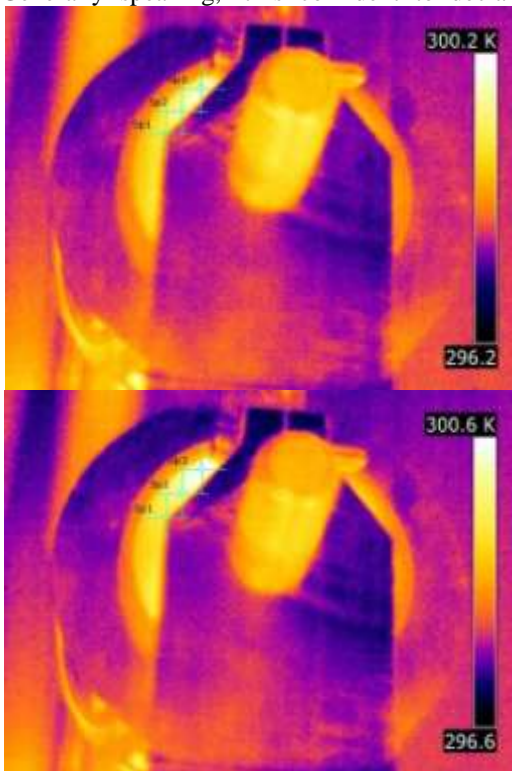
after 120s excitation at 10HZ and 1mm amplitude. To have the general distribution of temperature, six points are spotted in circumferential direction and the corresponding temperatures are listed in Table 2. Point 4 and 5 are symmetric over the horizontal line of the structure and displays same temperature. The maximum temperature appears at the top loading zone, which is close to the external surface of rubber core. As the spotted point is far away from the top loading zone, the temperature decreases gradually and reaches to lowest at the horizontal line. Even though the bottom part of the temperature is invisible, the symmetrical structure and the sinusoidal loading assure the symmetry of temperature distribution. Thus, the dynamic testing temperature distribution matches well with the simulation result. Furthermore after 120s, the simulation gives a maximum temperature 303K and the dynamic test gives a maximum temperature 302K. The slightly lower temperature in the dynamic testing can attribute to the heat transfer from the surface to ambient. Generally speaking, it is confident to declare the

reliability of Simplex program and FVM simulation in predicting the temperature distribution of rubber bushing.

Table 2: Temperature distribution on the surface of rubber bushing

Points No.	1	2	3	4	5	6
Temp(K)	303.0	302.5	300.8	300.7	300.7	300.9

Figure 14 shows a series of photos captured by the thermal imager at different time. Those photos are numbered from left to right and then from top to bottom. The maximum temperature changes from 300.2K to 301.9K in 100s. Temperature from three points are collected from each photo and plotted in Figure 15 to explore the heat concentration in rubber core.



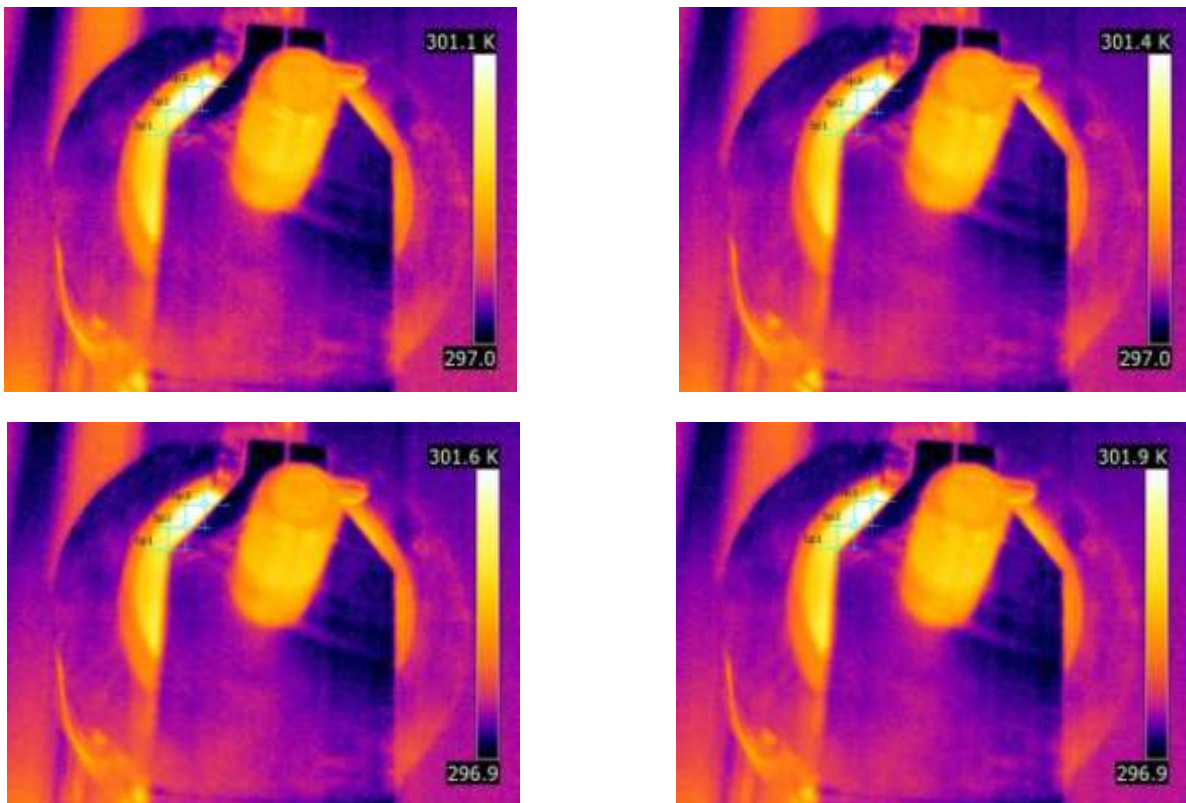


Figure 14. Temperature distribution on the surface of rubber core (a) $t=4s$; (b) $t=15s$; (c) $t=31s$; (d) $t=45s$; (e) $t=58s$; (f) $t=72s$; (g) $t=84s$; (h) $t=99s$.

sp3 is a point close to the top loading zone and has the higher temperature than the other two points. sp1 is a point close to the central horizontal line and has the lowest temperature. Figure 14 indicates the temperature gradient of rubber core in circumference becomes more and more evident. At the beginning, the temperature of the three points are pretty close, especially that at the points sp2 and sp3. During the cycle loading, the temperature at point sp1 increases much slower than that at the other two points. This quick temperature rising of point sp3 can attribute the higher heat generation rate in that area. Nevertheless, heat fast rising temperature make the top loading zone as the most easy damaged place of rubber bushing under the radial loading and that result is helpful to investigate the stability of this structure.

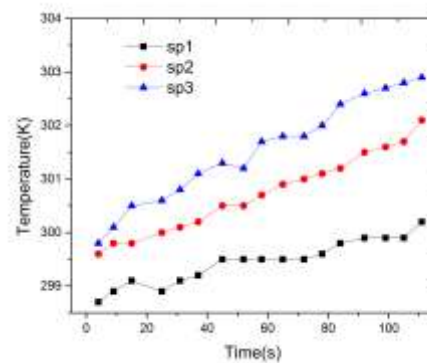


Figure 15. Rubber bushing surface temperature rising over time.

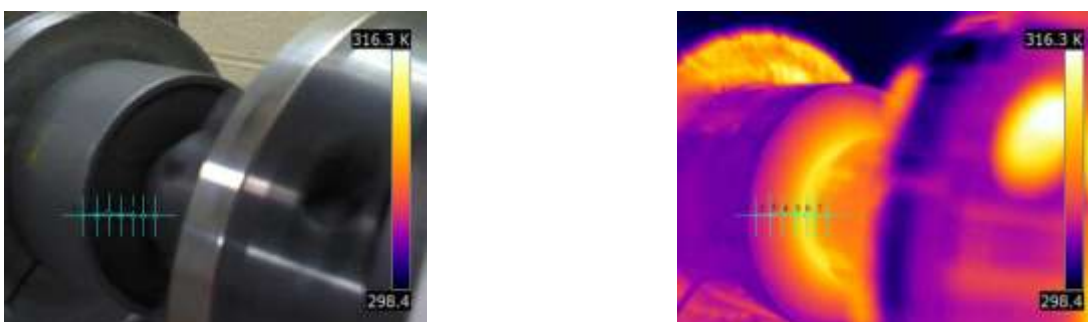


Figure 16. Temperature distribution of rubber bushing at torsional amplitude 5° and excitation frequency 10HZ (a) Digit camera; (b) thermal.

Table 3: Temperature distribution at torsional angle
 5° and 10HZ

Points No.	1	2	3	4	5	6	7
Temp (K)	303.2	304.8	306.4	309.1	311.4	309.0	307.5

Figure 16 is the digital photo and thermal photo recorded using thermal imager in order to explore the dynamic performance of rubber bushing under torsional testing. Torsional degree and frequency are specified as 5° and 10HZ respectively. Because the deformation under torsional degree 5° is relative larger than that under radial amplitude 1mm, the temperature rising under torsional test is quicker than that under the radial testing. Similarly, a group of points are spotted to explore the temperature distribution in radial direction. The locations of those points are clearer in the digital photo and the temperatures of selected points are list in Table 3. During the torsional test, the outer surface of the rubber core is fixed by the fixture and the torque is transmitted through the inner shaft. As a consequence, the points close to the inner shaft experience the higher deformation and have more dissipation energy accumulation. While in the circumferential direction, the deformation is uniform as the amplitude angle and radius determine the displacement. Finally, the inner surface zone of the rubber core becomes the concentration of heat built up and displays highest temperature. Point 6 is located on the interface of rubber and steel, thus, the temperature distribution in radial starts to decrease from this point. The thermal behavior of torsional testing identifies another easy failure zone of bushing as the inner surface of rubber core, where special attention is required for operation and design in future.

VI. Conclusion

The FEA program is developed to analyze the frequency dependent viscoelastic structure. In view of the out of phase between stress and strain, the dissipation energy density inside of the rubber component has been investigated. The principle and approach to calculate the external work, potential energy, kinetic energy and dissipation energy are elaborated and the clamped beam is practiced to verify the energy calculation with the principle of energy conservation. The periodicity of the dissipation energy under the harmonic excitation indicates the constant heat generation rate. The thermal properties are measured using TPS and the boundary condition of the heat transfer simulation is set to simulate the dynamic radial testing. The FVM allows different heat source at each control volume, and the heat generation of each volume comes from

the dissipation energy calculated from the Simplex program. To verify the accuracy and applicability of the Simplex program and following heat transfer simulation, dynamic radial testing is carried out. That results are recorded using indicates thermal imager and experimental temperature matches well with the simulated. The radial testing indicates that the higher temperature appears around vertical loading zone while the higher temperature at torsional testing appears at the central but close to the inner surface of the steel sleeves. Those results presents the easy failure zone of rubber bushing under different loading and shed a light on the design optimization.

Reference

- [1.] Kadowec, J., A. Wineman, and G. Hulbert, Elastomer bushing response: experiments and finite element modeling. *Acta mechanica*, 2003. 163(1-2): p. 25-38.
- [2.] Johnson, A.R. and T.-K. Chen, Approximating thermo-viscoelastic heating of largely strained solid rubber components. *Computer methods in applied mechanics and engineering*, 2005. 194(2): p. 313-325.
- [3.] Molinari, A. and Y. Germain, Self heating and thermal failure of polymers sustaining a compressive cyclic loading. *International journal of solids and structures*, 1996. 33(23): p. 3439-3462.
- [4.] Woo, C.S. and H.S. Park, Useful lifetime prediction of rubber component. *Engineering Failure Analysis*, 2011. 18(7): p. 1645-1651.
- [5.] Luchini, J., J. Peters, and R. Arthur, Tire rolling loss computation with the finite element method. *Tire Science and Technology*, 1994. 22(4): p. 206-222.
- [6.] Diani, J., B. Fayolle, and P. Gilormini, A review on the Mullins effect. *European Polymer Journal*, 2009. 45(3): p. 601-612.
- [7.] Mullins, L., Softening of rubber by deformation. *Rubber Chemistry and Technology*, 1969. 42(1): p. 339-362.
- [8.] Roland, C., Network recovery from uniaxial extension: I. Elastic equilibrium. *Rubber chemistry and technology*, 1989. 62(5): p. 863-879.
- [9.] Mars, W. and A. Fatemi, Factors that affect the fatigue life of rubber: a literature survey. *Rubber Chemistry and Technology*, 2004. 77(3): p. 391-412.
- [10.] Clark, S.K., Temperature rise times in pneumatic tires. *Tire Science and Technology*, 1976. 4(3): p. 181-189.
- [11.] Yeow, S., M. El-Sherbiny, and T. Newcomb, Thermal analysis of a tyre during rolling or sliding. *Wear*, 1978. 48(1): p. 157-171.

- [12.] Becker, A., et al., A material model for simulating the hysteretic behavior of filled rubber for rolling tires. *Tire Science and Technology*, 1998. 26(3): p. 132-148.
- [13.] Lin, Y.-J. and S.-J. Hwang, Temperature prediction of rolling tires by computer simulation. *Mathematics and Computers in Simulation*, 2004. 67(3): p. 235-249.
- [14.] Whicker, D., et al., Modeling tire deformation for power loss calculations. *Training*, 1981. 2014: p. 07-22.
- [15.] Whicker, D., et al., A thermomechanical approach to tire power loss modeling. *Tire Science and Technology*, 1981. 9(1): p. 3-18.
- [16.] Whicker, D., A.L. Browne, and D.J. Segalman, The structure and use of the GMR combined thermo-mechanical tire power loss model. *Training*, 1981. 2014: p. 07-22.
- [17.] Jones, D.I., *Handbook of viscoelastic vibration damping*. 2001: Wiley.
- [18.] Ebbott, T., et al., Tire temperature and rolling resistance prediction with finite element analysis. *Tire Science and Technology*, 1999. 27(1): p. 2-21.
- [19.] Mc Allen, J., A. Cuitino, and V. Sernas, Numerical investigation of the deformation characteristics and heat generation in pneumatic aircraft tires: Part II. Thermal modeling. *Finite Elements in Analysis and Design*, 1996. 23(2): p. 265-290.
- [20.] Doyle, J.F., *Viscoelastic Wave Propagation*. *Encyclopedia of Thermal Stresses*, 2014: p. 6462-6467.
- [21.] Park, D.M., et al., Heat generation of filled rubber vulcanizates and its relationship with vulcanizate network structures. *European polymer journal*, 2000. 36(11): p. 2429-2436.
- [22.] Zhang, H.H.Z., *Viscoelastic Parameter Identification based Structure-Thermal Analysis of Rubber Bushing*. *Global Journal of Researches In Engineering*, 2014. 14(3).
- [23.] Doyle, J.F., *Nonlinear Structural Dynamics Using FE Methods*. 2014: Cambridge University Press.
- [24.] Sternberg, E., *On the analysis of thermal stresses in visco-elastic solids*. 1963, DTIC Document.